AGU PUBLICATIONS

JGR

Journal of Geophysical Research: Earth Surface

RESEARCH ARTICLE

10.1002/2016JF004181

Key Points:
- Hydropotential suggests that upstream water would route around the sticky spot which lies on a local topographic high
- Bed conditions vary from soft deformable till at topographic lows to more consolidated stiffer till
- Observation of a debris-rich frozen-on ice 40 m above a basal channel

Correspondence to:
T. Luthra,
tyl5106@psu.edu

Citation:
Luthra, T., L. E. Peters, S. Anandakrishnan, R. B. Alley, N. Holschuh, and A. M. Smith (2017), Characteristics of the sticky spot of Kamb Ice Stream, West Antarctica, *J. Geophys. Res. Earth Surf.*, *122*, 641–653, doi:10.1002/2016JF004181.

Received 24 DEC 2016
Accepted 6 MAR 2017
Accepted article online 8 MAR 2017
Published online 21 MAR 2017

Characteristics of the sticky spot of Kamb Ice Stream, West Antarctica

Tarun Luthra[1], Leo E. Peters[2], Sridhar Anandakrishnan[1], Richard B. Alley[1], Nicholas Holschuh[1], and Andrew M. Smith[3]

[1]Department of Geosciences, and Earth and Environmental Systems Institute, Pennsylvania State University, University Park, Pennsylvania, USA, [2]Institute for Marine and Antarctic Studies, University of Tasmania, Hobart, Tasmania, Australia, [3]British Antarctic Survey, Cambridge, UK

Abstract Amplitude analysis of reflection seismic data reveals the presence of highly variable bed conditions under the main sticky spot and adjacent regions of the Kamb Ice Stream (formerly ice stream C). The sticky spot, which is a zone of bed that imparts high basal resistance to ice flow, is situated on a local topographic high composed of consolidated sediments or sedimentary rock. Any meltwater draining from upglacier along the base of the ice is routed around the sticky spot. The ice over the sticky spot includes, in at least some places, a seismically detectable basal layer containing a low concentration of debris, which locally thickens to 40 m over a topographic low in the bed. The ice-contact basal material ranges from dilated and highly porous to more-compacted and stiff, and perhaps locally frozen. The softer material is preferentially in topographic lows, but there is not a one-to-one correspondence between basal character and basal topography. We speculate that the 40 m thick frozen-on debris layer formed by glaciohydraulic supercooling of lake-drainage events along a basal channel during the former, active phase of the ice stream. We also speculate that loss of lubricating water, perhaps from piracy upstream, contributed to the slowdown of the ice stream, with drag from the sticky spot playing an important role, and with the basal heterogeneity greatly increasing after the slowdown of the ice stream.

1. Introduction

Ice streams are important in draining mass from the West Antarctic Ice Sheet (WAIS) to the ocean, and their imbalances contribute to sea level change [*Jacobel et al.*, 2009; *Joughin and Alley*, 2011; *Joughin et al.*, 2014]. The fast flow of ice streams is attained mainly through basal sliding and active deformation of subglacial sediments [e.g., *Bentley*, 1987], so it is important to understand the basal mechanisms that control ice stream flow in order to predict the future of WAIS.

Ice streams often change rapidly [*Bennett*, 2003]. Some sectors of the WAIS have been losing mass through faster ice stream flow [*Shepherd et al.*, 2012]. The glaciers of the Amundsen Sea Embayment, some of which have high velocities at the grounding line and relatively small ice shelves to provide buttressing, have especially contributed to recent WAIS mass loss [*Jacobs et al.*, 2011; *Mouginot et al.*, 2014; *Rignot et al.*, 2008; *Shepherd et al.*, 2012]. However, two ice streams draining into the Ross Ice Shelf have shown the opposite trend; Whillans Ice Stream (WIS—formerly ice stream B) has decelerated in the last few decades, and Kamb Ice Stream (KIS—formerly ice stream C) almost completely stagnated about 150 years ago, shifting from velocities high enough to open abundant surface crevasses (>120 m a^{-1}) to its current slow speed of <10 m a^{-1} [*Anandakrishnan and Alley*, 1997b; *Joughin et al.*, 2005; *Retzlaff and Bentley*, 1993; *Joughin et al.*, 2002]. The slowdown of WIS and KIS has contributed to a local positive mass balance in the Ross Sea Sector of WAIS [*Rignot et al.*, 2008]. This may represent part of a longer-term trend [*Bindschadler et al.*, 1990], or may result from century-scale flow oscillations [*Hulbe and Fahnestock*, 2007; *Bougamont et al.*, 2015; *Robel et al.*, 2014; *van der Wel et al.*, 2013], or both.

The rapid flow of the West Antarctic ice streams draining into the Ross Ice Shelf (the so-called Siple Coast ice streams, which move at up to 400 m a^{-1}) is achieved by deformation within or sliding over a wet deformable subglacial bed [*Alley et al.*, 1986, 1987; *Blankenship et al.*, 1986; *Kamb*, 2001; *Tulaczyk et al.*, 2000]. Hypotheses for the slowdown of WIS and KIS thus generally focus on changes in the bed [e.g., *Anandakrishnan and Alley*, 1997b; *Tulaczyk et al.*, 2000; *Winberry et al.*, 2014].

Focusing on KIS here, hypotheses have generally involved loss of lubrication through some combination of drainage diversion, drainage concentration, or basal freeze-on, leading to formation, expansion, or increased

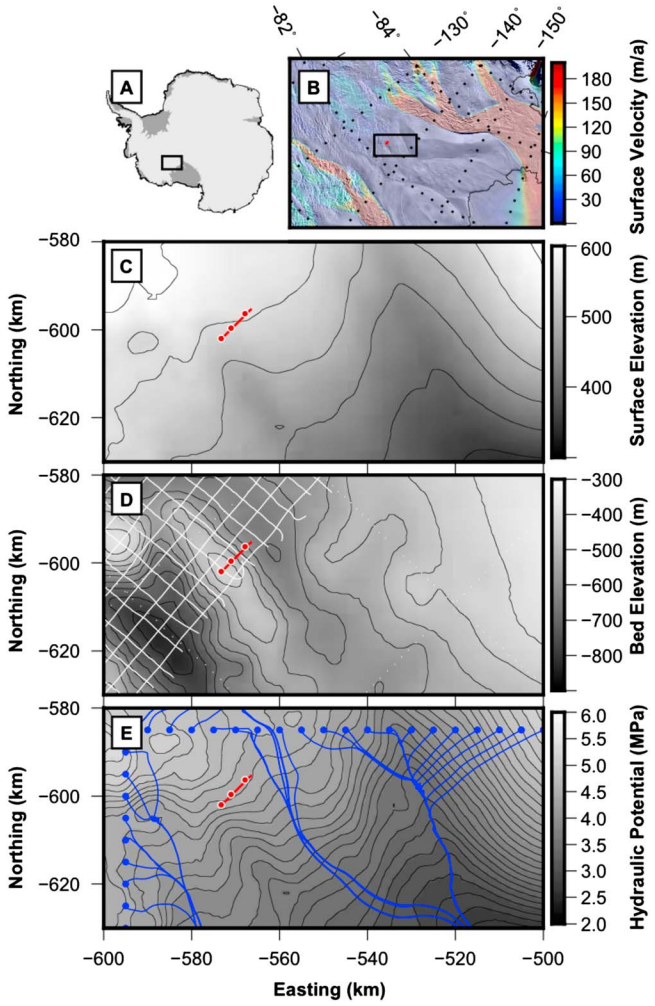

Figure 1. (a) Location of Kamb Ice Stream seismic profile. (b) Ice-flow velocity of KIS [*Rignot et al.*, 2011]. (c) Surface elevation map with location of seismic line. (d) Bed elevation map and the bed map data grid lines used to derive the hydrologic potential flow lines, and the seismic profile (red line), which is oriented transverse to ice stream flow; the blue circles show the *Engelhardt* [2004] borehole sites. The box in Figure 1b shows the location of Figures 1c and 1d. (e) As in Figure 1c but showing the hydrologic potential.

friction on "sticky spots" [*Alley*, 1993; *Anandakrishnan and Alley*, 1994; *Anandakrishnan and Bentley*, 1993; *Anandakrishnan and Alley*, 1997a; *Anandakrishnan et al.*, 2001] while still leaving some basal water in places beneath the ice stream [*Atre and Bentley*, 1993; *Bentley et al.*, 1998; *Catania et al.*, 2003; *Engelhardt*, 2004; *Kamb*, 2001]. Diversion of water from KIS to WIS ("water piracy") was suggested as a mechanism to reduce the available water for KIS [*Alley et al.*, 1994; *Anandakrishnan and Alley*, 1997b]. *Engelhardt* [2004] suggested that wet basal conditions are primarily confined to relatively narrow and localized water channels present beneath the ice stream; changes in channelization may then have been important. Borehole data and heat-flow estimates show that freeze-on occurs beneath KIS [*Joughin et al.*, 2003; *Christoffersen et al.*, 2010], such that lubricating water decreases along flow; a time-trend to increasing freeze-on perhaps from the long-term evolution in response to the end of the last ice age may have contributed to the slowdown.

Several authors have proposed that reactivation of KIS is possible [*Bougamont et al.*, 2003; *Jacobel et al.*, 2009; *Vogel et al.*, 2005]. Wet basal conditions exist in certain sections along KIS [*Catania et al.*, 2003; *Engelhardt*, 2004; *Peters and Anandakrishnan*, 2007], and a large bulge is growing where still-active tributary flow reaches the stagnant main body of KIS [*Alley et al.*, 1994; *Price et al.*, 2001; *Joughin et al.*, 2002], which might propagate downglacier and reactivate the ice stream [*Vogel et al.*, 2005; *Engelhardt and Kamb*, 2013; *Bougamont et al.*, 2015]. Questions about causes of the KIS shutdown and possible reversal likely will be answered by additional modeling, which must be guided by data addressing the key conditions and processes.

To contribute to this effort, here we present the results of a seismic reflection experiment performed across a prominent feature on the main trunk of KIS that we refer to as a "sticky spot" (Figure 1). The feature appears prominently in satellite imagery as a teardrop-shaped feature with ice flow lines diverging around it, suggesting that basal conditions differ between it and the surrounding ice stream, and possibly differed when the ice stream was active. We note that this feature of KIS is similar in many ways to "ice rise a" of the ice plain of adjacent Whillans Ice Stream and likely exists in a continuum of features, including ice rises in ice shelves, with elevated beds and locally higher resistance to flow [*Matsuoka et al.*, 2015; *Halberstadt et al.*, 2016]. To understand this basal feature of KIS, our reflection seismic line was oriented transverse to ice flow crossing from the sticky spot onto the adjacent ice stream (Figure 1). We conducted a seismic amplitude analysis to estimate basal conditions along the line.

Consistent with and extending local borehole observations [*Kamb*, 2001; *Engelhardt*, 2004], we find that basal conditions now are notably variable both on the sticky spot and on the surrounding ice stream, with some regions of thawed and potentially deformable bed, while others are more consolidated or frozen. There are suggestions that the sticky spot was more variable than the surroundings when the ice stream was active. Furthermore, our seismic results suggest that basal water has frozen onto the base of the glacier, primarily within distinct subglacial channels, one of which appears to still contain thawed subglacial sediments.

2. Kamb Ice Stream Stagnation and Present Bed Condition

As noted above, the Siple Coast ice streams move rapidly by sliding over or deforming a layer of water-saturated soft sediments in which pore water pressures are high [*Alley et al.*, 1986; *Blankenship et al.*, 1986; *Kamb*, 2001]. Small changes in bed properties may lead to slower basal motion, thus slowing the ice stream, as has occurred for KIS and is occurring for WIS [*Anandakrishnan et al.*, 2001; *Bindschadler et al.*, 1996; *Luthra et al.*, 2016].

Several geophysical studies have documented a soft, well-lubricated bed beneath parts of KIS, which would favor fast ice flow as in adjacent ice streams, but with KIS having some less-lubricated regions and generally greater spatial heterogeneity than adjacent ice streams [*Atre and Bentley*, 1993; *Bentley et al.*, 1998; *Catania et al.*, 2003]. *Atre and Bentley* [1993] interpreted their seismic reflection data as indicating regions of both unconsolidated dilated sediments and stiffer, more-consolidated sediments on KIS. *Peters and Anandakrishnan* [2007] performed a seismic amplitude analysis along a survey line oriented transverse to KIS about 30 km upstream of the sticky spot and found spatial heterogeneity with both dilatant and frozen bed conditions. Extensive radar analyses conducted by *Catania et al.* [2003] and *Jacobel et al.* [2009] concurred with the seismic and borehole work that portions of the bed of KIS are thawed, with the exception of the sticky spot that is likely frozen. Thus, portions of the bed of KIS remain favorable for fast flow and could contribute to reactivation in the future [*Vogel et al.*, 2005], but these well-lubricated conditions are not spatially continuous across the ice stream, and the sticky spot is especially prominent.

Low effective pressure (the difference between the ice-overburden pressure and the water pressure at the base of the ice) in a basal water system is typically associated with fast ice stream flow and is observed on both WIS and Bindschadler Ice Stream (BIS) [*Blankenship et al.*, 1987; *Blankenship et al.*, 1986; *Kamb*, 2001]. *Kamb* [2001] also observed low effective pressure in parts of KIS from the borehole analyses. *Engelhardt* [2004] reported data from boreholes near and on the sticky spot upstream of our seismic line (Figure 1). A borehole on the sticky spot encountered a frozen bed; water did not drain easily from the bottom of the borehole. Another, in the former ice stream away from the sticky spot, connected rapidly to a basal water system. Of two boreholes near the margin of the sticky spot, one penetrated a 1.4 m deepwater body (Figure 1), whereas the other connected to a water system after a delay suggesting some degree of freeze-on. This heterogeneity may be important, as discussed below.

Analyses of till from beneath the ice streams showed many similarities, but some differences that may be important. Measured mean till porosity was similar beneath KIS, WIS, and BIS, but KIS had more variability with a lower minimum porosity [*Kamb*, 2001]. Also, the maximum till strength on KIS was considerably higher than that of till beneath WIS [*Kamb*, 2001].

The data remain sparse and somewhat noisy. In general, though, they indicate greater spatial heterogeneity beneath KIS than beneath adjacent ice streams, with some regions still well lubricated but others much less so.

3. Seismic Data Collection and Processing

A 10 km long multichannel seismic reflection profile was collected across the southern margin of the main sticky spot of KIS during the 2002–2003 Antarctic field season (Figure 1). As noted above, this sticky spot is a prominent feature in satellite imagery, appearing as a teardrop shape with flow lines diverging to either side (Figure 1). The seismic line was oriented perpendicular to ice flow in order to image and quantify the subglacial properties along the line and compare conditions beneath the teardrop and beneath the streamlines. The seismic experiment was conducted near the location of boreholes drilled by *Engelhardt* [2004] beneath the KIS (Figure 1c).

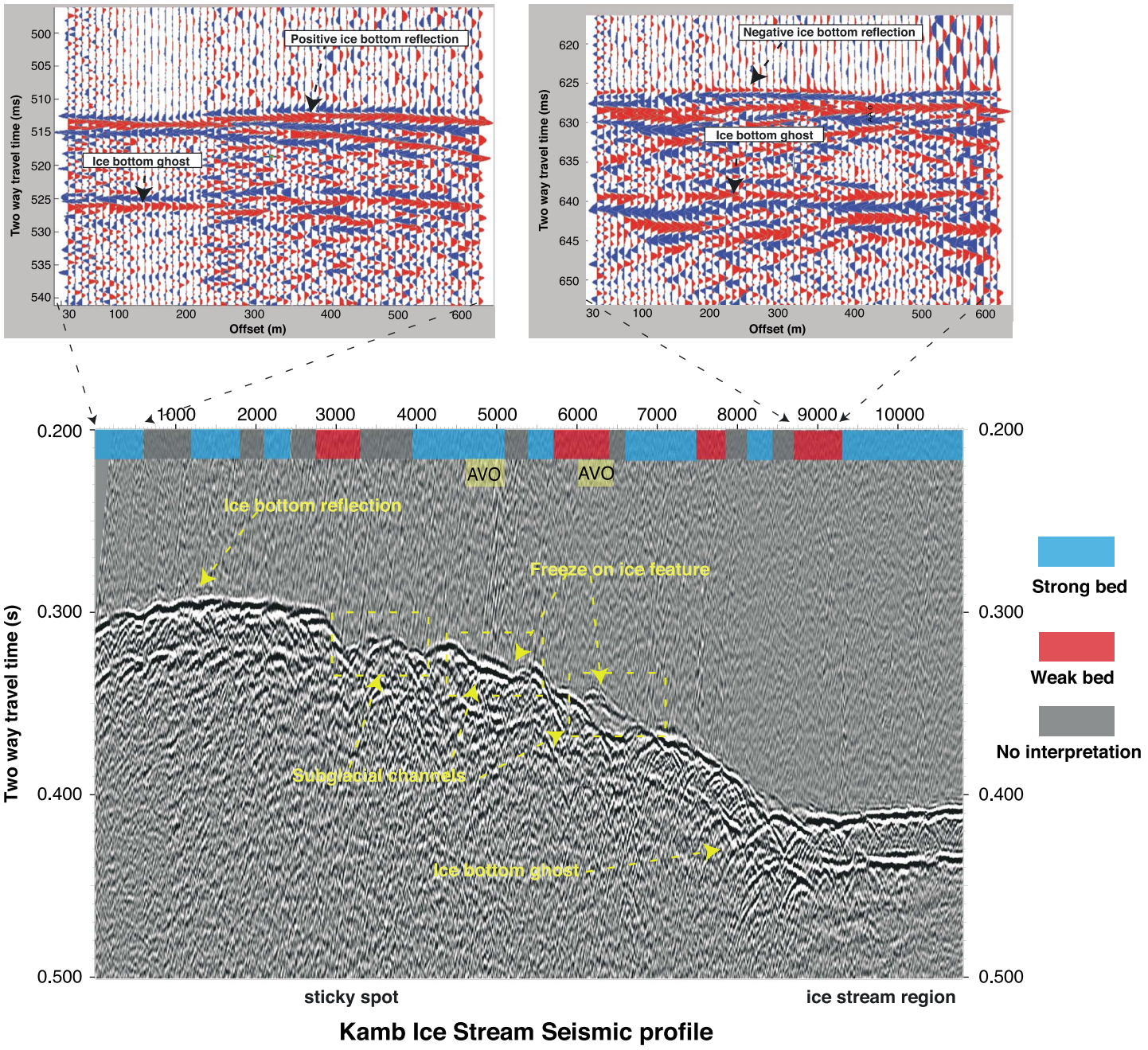

Figure 2. Seismic profile of Kamb Ice Stream. The blue and red boxes indicate strong and weak bed conditions based on the reflectivity analysis. The yellow box marks the AVO analysis zones. The inset (top) shows that NMO-corrected shot gathers depicting polarity shifts across the line.

We deployed a receiver array of 120 geophones at 10 m spacing for the 2-D seismic profiling. Sources were detonated at distances of 30 m and 1230 m from the end of the array, resulting in reflection data with source-to-receiver distances that ranged from 30 m to 2420 m. The entire source-receiver array was then moved 300 m and the source detonations were repeated, resulting in a data set in which subsurface points were imaged multiple times at different incidence angles. Explosive charges ranged from 150 g to 900 g in size and were detonated in holes drilled to ~20 m depth by using a hot water drill. The receivers were buried approximately 0.5 m below the surface to reduce surface noise and improve the signal-to-noise ratios (SNR).

Standard multichannel processing techniques were applied to generate an image of the seismic profile (Figure 2). A predictive deconvolution operator was used to reduce the strength of the so-called ghost

reflection that is observed in the data about 20 ms after the ice bottom reflection. The ghost reflection arises from the energy that reflects off the surface of the ice immediately after a shot, and then travels downward through the ice sheet, and is delayed by a small amount relative to the energy that travels directly downward. Bandpass and frequency-wave number (FK) filtering were used to remove energy from the direct wave arrivals (energy that travels along the surface directly from source to receiver) and other surface waves (air waves and multiply reflected trapped energy in the firn) that interfere with the ice bottom reflection. The primary energy of the seismic data peaks at frequencies of ~150 Hz, which would generate a vertical resolution of approximately 6.5 m in ice. Finer vertical resolution is obtained for this frequency in the lower velocity materials likely to exist beneath the ice (water $V_p = 1500\ \mathrm{m\ s^{-1}}$, resolution = 2.5 m; unconsolidated sediments $V_p = 1550$–$2100\ \mathrm{m\ s^{-1}}$, resolution = 2.5–3.5 m; and consolidated sediments $V_p = 2200$–$3000\ \mathrm{m\ s^{-1}}$, resolution = 3.5–5 m).

We applied static corrections to adjust for the variations in the shot hole depths and for surface topography. After filtering, editing bad traces, and correcting for known sources of timing errors, the seismic data were corrected for the distance between the source and receiver (the so-called normal moveout correction or NMO). These NMO-corrected data for a source-receiver pair are equivalent to a seismic record taken with the source and receiver at the same location (zero-offset) if our knowledge of seismic velocities is accurate. The NMO-corrected traces for reflections off common points at the bed were then summed in order to improve the signal-to-noise ratio. The final outcome is a so-called common-midpoint stack, in which each trace is a zero-offset reflection record at 5 m spacing along the line.

4. Seismic Amplitude Analysis

The polarity and amplitude of a seismic reflection depend on the contrast in elastic properties (compressional or *P* wave velocity, V_p; shear or *S* wave velocity, V_s, and density, ρ) across an interface [*Aki and Richards*, 2002]. In glacial environments, the nature of the subglacial material can be diagnosed by variation in reflector amplitude across a range of source-to-receiver offsets, together with the known properties of the ice [*Anandakrishnan*, 2003]. The observed displacement amplitude A recorded at a geophone from a seismic wave that reflects off an interface is given by [e.g., *Peters et al.*, 2008]

$$A(\theta_i) = A_0 R(\theta_i)\gamma(\theta_i)e^{-ar(\theta_i)}. \tag{1}$$

Equation (1) shows that for a given incidence angle θ_i, A is a function of the source amplitude (A_0); the reflection coefficient for the interface, (R); geometric spreading losses (γ); and attenuation losses (a) along the path length (r) from source to receiver. The contrast in elastic properties across the reflection interface controls $R(\theta_i)$ [*Aki and Richards*, 2002]. Thus, the reflectivity $R(\theta_i)$ off the ice bottom can be used to estimate properties of the subglacial layer if ice properties are known [*Peters et al.*, 2008].

At normal incidence, the *P* wave reflectivity is a function of the acoustic impedances Z_i of the layers on either side of the interface:

$$R_0 = \frac{Z_2 - Z_1}{Z_2 + Z_1} \tag{2}$$

The indices "1" and "2" refer to the upper and lower media, where $Z_i = \rho_i V_p$ is the acoustic impedance in the ith layer. At an ice-subglacial bed interface, more competent sediments and crystalline basement have higher acoustic impedance than ice ($R_0 > 0$), whereas water and water-rich sediments including high-porosity till typically have a lower impedance than ice ($R_0 < 0$).

We note that the sign of the reflection coefficient does not uniquely identify the subglacial material; however, numerous prior studies on KIS and adjacent ice streams [e.g., *Atre and Bentley*, 1993; *Blankenship et al.*, 1986, 1987; *Peters and Anandakrishnan*, 2007], and especially those studies involving direct drilling [e.g., *Christoffersen et al.*, 2010; *Engelhardt*, 2004; *Engelhardt and Kamb*, 2013; *Kamb*, 2001], provide high confidence that reflections with $R_o < 0$ arise from unconsolidated, water-saturated, dilated, and likely deforming subglacial sediments with high water pressure (low effective pressure) or from lakes. We do not find evidence for extensive lakes here, nor have other investigators [e.g., *Fricker et al.*, 2016, and references therein], so we refer to regions with $R_o < 0$ as "soft beds," and to regions with $R_o > 0$ as "hard beds," which may include relatively compacted tills and more consolidated rocks. We note that $R_o \sim 0$ (±0.1) likely arises from a till intermediate between "soft" dilated-deforming and "hard" compacted-lodged [*Peters et al.*, 2007] (also see *Leeman et al.*

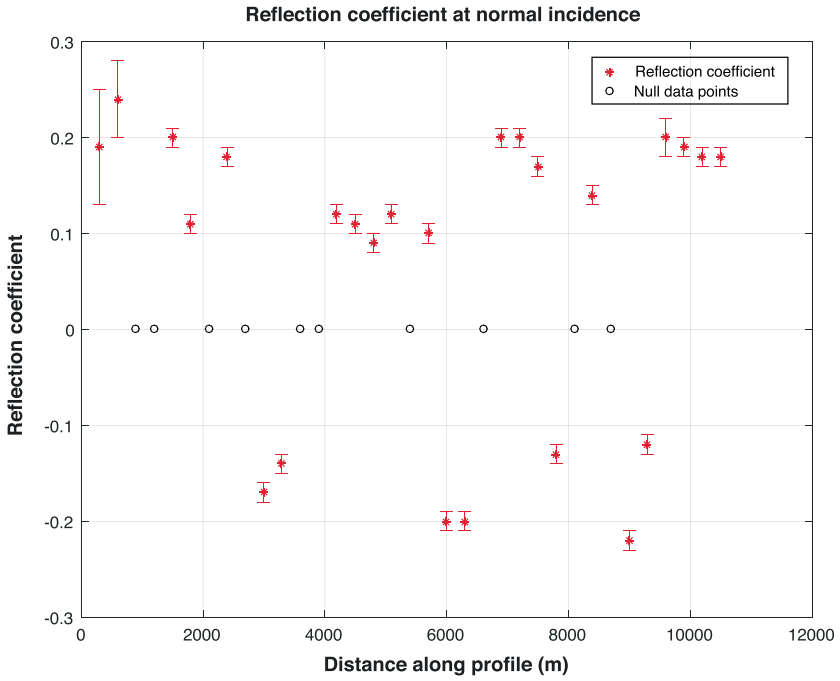

Figure 3. Basal reflection coefficient at normal incidence across the seismic profile with uncertainty (1-sigma). Those reflections that were not clear enough to allow confident quantification of the amplitude and phase are plotted as black circles at zero reflection coefficient.

[2016], as well as *Rathbun et al.* [2008], which update and extend relations among till strength, porosity, permeability, and other geotechnical properties, and *Iverson and Zoet* [2016, and references therein] for additional insights on till deformation). As discussed below, we confirm and extend this assumption by using amplitude variation with offset seismic experiments for selected parts of our seismic line, which indirectly incorporate information from shear waves because of conversions between compressional and shear waves during nonnormal-incidence reflection and transmission at the basal interface.

We first used the normal-incidence seismic data set to measure reflectivity changes along the seismic profile (Figure 3). The reflection coefficient is nearly constant for angles of incidence less that 10°. Further, the raypath lengths are nearly identical, allowing us to interpret all seismic traces with $\theta_i < 10°$ as if they were at normal incidence. This method has been successfully used in the past to constrain estimates of the character of the subglacial bed beneath various regions of the WAIS [*Atre and Bentley*, 1993; *Bentley*, 1971; *Roethlisberger*, 1972; *Smith*, 1997]. Following the approach of *Holland and Anandakrishnan* [2009], we estimated the normal-incidence reflection coefficient as

$$R_0 = 2\frac{A_2}{A_1}e^{2aH} \tag{3}$$

where A_1 and A_2 are the primary and multiple reflection amplitudes, respectively; H is the thickness of the ice column; and a is the attenuation in ice. The multiple reflection is energy that has made two round trips from surface to bed and back to the surface. Here the ratio of A_1 and A_2 removes the A_0 term in equation (1), since both reflections emanate from the same source. The attenuation "a" is internal friction within the ice (we take $a = 0.2\,\mathrm{km}^{-1}$ [from *Bentley and Kohnen*, 1976]), and H is the ice thickness (e^{2aH} accounts for reduction in observed amplitude due to loss of energy within the ice column). The SNR for A_1 was estimated by comparing the peak reflection amplitude to the energy in a 5 ms window before the reflection (an estimate of background noise), thus providing uncertainties in the signal. We excluded receiver amplitudes that were contaminated with noise from the surface waves.

Although normal-incidence amplitude analysis provides important information on subglacial conditions, it has limitations. The reflection coefficient at normal incidence depends only on the impedance contrast across the interface between the two layers, and it is not possible to separate the contributions of seismic velocity

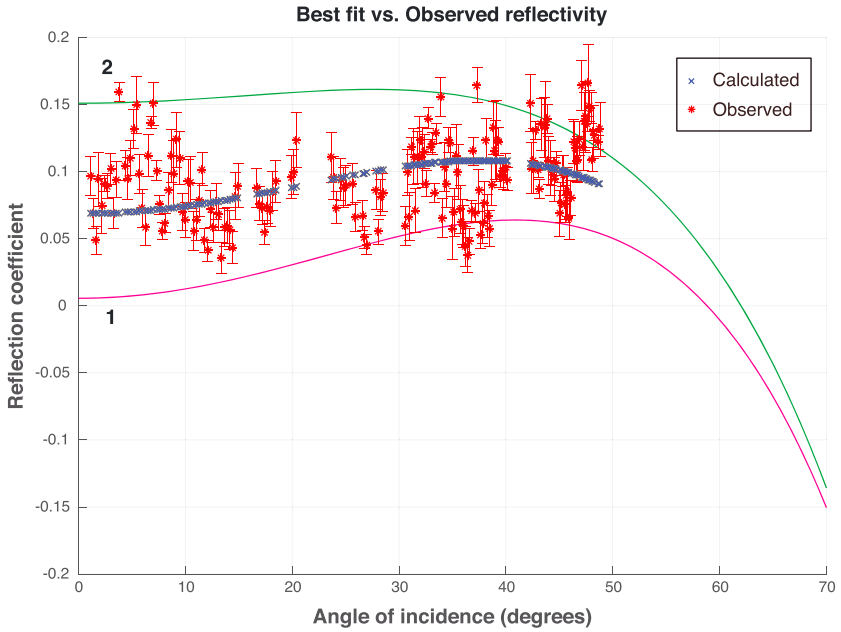

Figure 4. Basal reflection coefficient and uncertainty (1-sigma) against incidence angle, for section from 4600 to 4900 m. The blue line shows the least squares fit for the observed reflection coefficients ($V_p = 2090$ m s^{-1}, $V_s = 475$ m s^{-1}, density = 1950 kg m^{-3}). To illustrate the sensitivity of the inversion to the parameters, lines 1 and 2 are forward model curves based on the Zoeppritz equations: 1. $V_p = 1900$ m s^{-1}, $V_s = 450$ m s^{-1}, density = 1900 kg m^{-3}; 2. $V_p = 2200$ m s^{-1}, $V_s = 600$ m s^{-1}, density = 2200 kg m^{-3}).

and density. Furthermore, R_0 does not include information about the *S* wave velocity of the bed, because there is no conversion from compressional to shear waves at normal incidence. (Our explosive sources do not generate much *S* wave energy, so we cannot conduct a similar analysis by using incident *S* waves.)

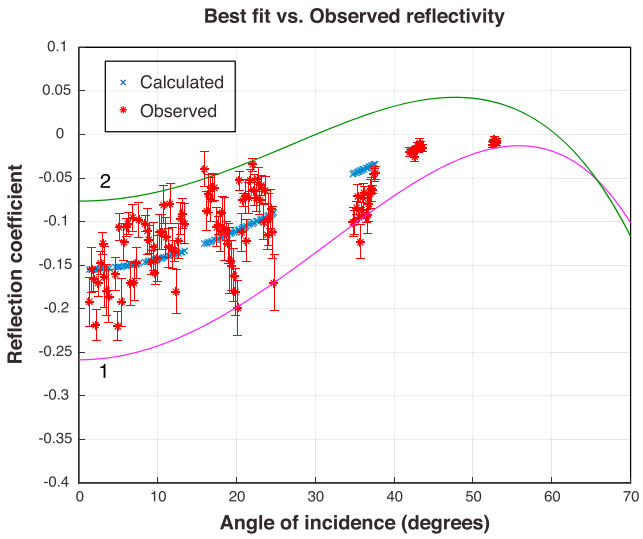

Figure 5. Basal reflection coefficient and uncertainty (1-sigma) against incidence angle, for section from 6000 to 6300 m. The blue line shows the least squares fit for the observed reflection coefficients ($V_p = 1550$ m s^{-1}, $V_s = 250$ m s^{-1}, density = 1680 kg m^{-3}). To illustrate sensitivity of the inversion to the parameters, lines 1 and 2 are forward model curves based on the Zoeppritz equations: 1. $V_p = 1500$ m s^{-1}, $V_s = 150$ m s^{-1}, density = 1500 kg m^{-3}; 2. $V_p = 1840$ m s^{-1}, $V_s = 300$ m s^{-1}, density = 1830 kg m^{-3}).

To further characterize the subglacial system, partially overcoming these difficulties, we performed amplitude variation with offset (AVO) analysis on two 300 m long sections of the bed (Figure 2), following the technique applied by *Peters et al.* [2008] and *Luthra et al.* [2016]. (Practical constraints prevented application of the technique along the entire line.) All the reflection points in a section were analyzed together, under the assumption that the subglacial properties do not change significantly within a 300 m footprint, and informed by the lack of major change in the vertical-incidence data. This allows us to analyze a range of incidence angles from 0 to 50°. The properties of the ice were estimated from the seismic data (the NMO correction provides an accurate measure of velocity in the ice), using tabulated values for the density of ice (with some corrections for possible

Table 1. Seismic Properties of the Till Inferred From AVO Analysis With Uncertainty (1-Sigma)[a]

Section (m)	4600–4900 (best fit)	4600–4900 (upper)	4600–4900 (lower)	6000–6300 (best fit)	6000–6300 (upper)	6000–6300 (lower)
V_p (m s^{-1})	2090 ± 200	2200	1900	1550 ± 200	1840	1500
V_s (m s^{-1})	475 ± 80	600	450	250 ± 50	300	150
Density (kg m^{-3})	1950 ± 190	2200	1900	1680 ± 200	1830	1500

[a]Upper and lower values refer to the forward model curves on the AVO plots. Ice velocities of $V_p = 3880$ (m s^{-1}), $V_s = 1860$ (m s^{-1}), density = 920 (kg m^{-3}) were used in the model.

entrained sediments—see section 5). We measured reflection amplitudes and estimated reflection coefficients at those angles. We used a least squares minimization technique to determine the elastic properties of the subglacial bed that best fit our estimates of the reflection coefficient (Figures 4 and 5). The best fitting elastic properties, along with the elastic properties of ice that were used in the inversion, are listed in Table 1.

As discussed in prior work such as *Blankenship et al.* [1986, 1987], shear waves provide sensitive probes for effective pressure in subglacial granular materials, and thus for porosity and dilatancy of the till. The converted shear waves also provide higher vertical resolution because of their lower velocity than that of compressional waves. We note, however, that due to the dominant wavelength of the seismic data, we cannot resolve layers thinner than ~1 m, and our interpretations are guided by knowledge of the subglacial environment informed by borehole studies, laboratory experiments, and modeling.

5. Seismic Results and Interpretation

A spatially heterogeneous subglacial bed is observed across the sticky spot, ranging from dilatant till (which is favorable for fast ice flow), to frozen or lithified sediments (inhibiting fast flow). This is in agreement with inferences from previous radar studies [*Atre and Bentley*, 1993; *Bentley et al.*, 1998; *Catania et al.*, 2003]. This is shown clearly by the phase of the seismic reflection from the bed, which is negative in some regions ($R < 0$; weak/soft beds), interspersed with regions of positive reflection phase ($R > 0$; stiff/stronger bed) (Figure 2).

Normal-incidence amplitude analysis reveals the reflectivity, and thus the contrast in material properties, along the seismic profile (Figure 3). Each data point in Figure 3 represents average conditions for a 70 m long section of the bed, and the centers of these sections are 300 m apart for adjacent data points. Weak or inconsistent reflections in some sections made it difficult or impossible to estimate the reflection coefficient accurately, as shown in Figure 3. The data show a bed with a "strong" mode (reflection coefficient ~ 0.15) and a "weak" mode (reflection coefficient ~ −0.15). Transitions between these occur over short distances, in some places in the ~230 m gap between the closest ends of adjacent imaged areas of the bed.

The normal-incidence amplitude analysis reveals that the sticky spot, in general, has the characteristics of a relatively strong bed, with measured reflectivity values typically 0.15–0.2 (Figure 3). However, distinct patches of weaker bed conditions are also observed across this region (e.g., sections 2400–3900 m and 5700–6300 m). These weak-bed sections are preferentially located in topographic troughs along the profile. Furthermore, the bed is relatively weak at the margin of the sticky spot and extending out into the ice stream (section 8400–9300 m).

The sticky spot is a large topographic high, but there is notable topography at shorter wavelengths. Topographic lows centered near 3300 m and 6500 m may be channels oriented across our seismic line and thus more-or-less along the direction of flow when the ice stream was active. (Note that the additional shallower reflector near 6500 m is likely a contact between dirtier and cleaner ice, as discussed below.) The topographic low near 3300 m is soft-bedded, and although there is a slight spatial offset, this is probably also true of the low near 6500 m. Well away from the sticky spot, in the flat-bedded portion of the ice stream (section 9300–10,500 m), the reflectivity indicates a stronger bed.

The two AVO analyses found contrasting subglacial bed properties (Figures 4 and 5 and Table 1). Both regions showed a weak reflector above the main reflector; we interpret this weak reflector as the contact between clean englacial ice and debris-bearing "dirty" basal ice. The borehole observations showed that KIS has

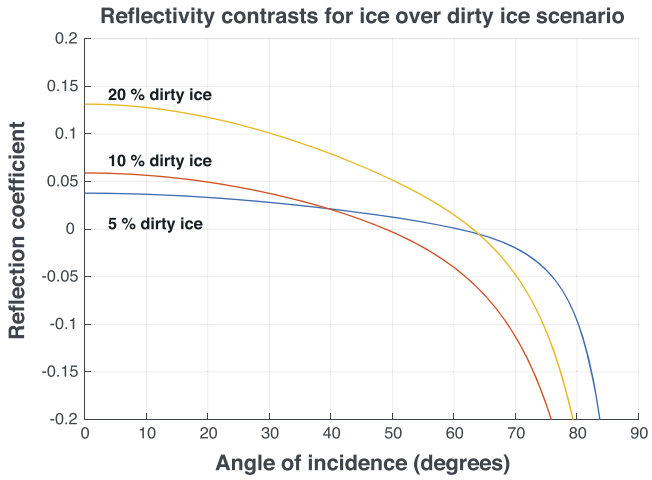

Figure 6. Forward model illustrating the reflectivity contrasts for a clean ice over dirty ice contact of 5, 10, and 20%. A 5% dirty ice contact produces a faint reflection coefficient across the incidence angle and will make an insignificant change to the overall bed properties. However, the 10–20% dirty ice case generates a relatively strong reflectivity and if unaccounted can significantly misrepresent the seismic properties at the bed.

several meters of dirty basal ice [*Kamb*, 2001; *Christoffersen et al.*, 2010], which might be detected by the normal-incidence surveys but is more easily characterized in the AVO; we return to this below.

The main basal reflector in the AVO section 4600–4900 m shows a consistent positive reflection for all incidence angles. AVO is sensitive primarily to the contrast between the two layers. We have generated two models that we consider to be most consistent with the data and our understanding of the setting: (1) ice with low debris concentration overlying a layer of sediments with relatively low porosity or (2) ice with low debris concentration overlying ice with high debris concentration. We prefer the former model mainly because in case (2) we would expect to see, but do not, an additional reflector from the contact between the debris-laden ice and the thawed till or bedrock beneath it. While the absence of evidence does not rule out model (2), we consider model (1) to be more likely because of its similarity to other regions of the ice stream. (Below, we discuss the region from 6000 to 6300 m, where there is evidence for a three-layer (ice/dirty-ice/sediments) basal environment.) Assuming model (1), with nearly clean ice over a sedimentary layer, we estimate that the sediment is relatively well consolidated ($V_p = 2100\,\mathrm{m\,s^{-1}}$, $V_s = 480\,\mathrm{m\,s^{-1}}$, *density* $= 1980\,\mathrm{kg\,m^{-3}}$; Table 1). We note that our data, and this model, do not exclude a layer of ice with high debris concentration between the low-debris-concentration ice and the well-consolidated sediments, but that is too thin to resolve seismically.

In contrast, the main reflector in the channel at 6000–6300 m has a negative polarity with weak reflection strength at all incidence angles, suggesting the presence of thawed, dilated sediments. In this region, we more clearly observe an englacial reflector, which we interpret as the top of a layer of sediment-laden ice [*Engelhardt*, 2004]. The layer is approximately 40 m thick at its thickest point, a large value that we discuss below.

In the calculations above, we assumed the seismic properties of clean ice for materials above the main basal reflector. However, the borehole observations of *Engelhardt* [2004] and our seismic observations suggest that clean ice overlies dirty ice that is thick enough to be resolved seismically, and this dirty ice overlies the bed. If so, then the bed may have a slightly greater acoustic impedance than we have estimated, because the overlying ice has a higher density and a slightly lower seismic velocities than we have assumed [*Bentley*, 1972]. In principle, we could apply AVO to the clean ice/dirty ice contact to determine the debris concentration of the dirty ice, and then use that result at the deeper interface to accurately estimate subglacial properties. However, the clean ice/dirty ice reflector is weak with poor SNR, precluding quantitative estimates of ice properties.

In Figure 6, we show the calculated reflection strength from an interface with clean ice over dirty ice containing 5%, 10%, or 20% debris by weight. For concentrations of ~10% or above, we estimate that the reflection from a seismically thick layer would be strong enough for useful application of AVO. Because we see a clean ice/dirty ice reflector but cannot characterize it accurately, we estimate that the debris concentration is ~5% in the dirty ice resolved by our seismic experiment, although with notable uncertainties. (Thin layers of debris-rich ice with higher concentrations may be present but not resolved [*Christoffersen et al.*, 2010].)

To assess the possible effects of this dirty ice layer on the inversion for sediment properties, we repeated the AVO models assuming that the upper layer is dirty ice containing either 5%, 10%, or 20% debris by weight

Table 2. Effect of Dirty Basal Ice on Best Fit Model Results[a]

	Section 4600–4900			Section 6000–6300		
	Best Fit V_p ($m\,s^{-1}$)	Best Fit V_s ($m\,s^{-1}$)	Best Fit Density ($kg\,m^{-3}$)	Best Fit V_p ($m\,s^{-1}$)	Best Fit V_s ($m\,s^{-1}$)	Best Fit Density ($kg\,m^{-3}$)
Clean ice	2400	612	1700	1550	255	1687
Dirty ice (10% sediment, density = 1080 $kg\,m^{-3}$)	2400	612	1990	1550	255	1980
Dirty ice (20% sediment, density = 1230 $kg\,m^{-3}$)	2400	612	2270	1905	368	1838

[a]For section 4600–4900, the range for V_p = 1500–2400 ($m\,s^{-1}$), V_s = 400–1000 ($m\,s^{-1}$), and density = 1500–2400 ($kg\,m^{-3}$). For section 6000–6300, the range for V_p = 1500–2000 ($m\,s^{-1}$), V_s = 50–500 ($m\,s^{-1}$), and density = 1500–2000 ($kg\,m^{-3}$). The ice elastic properties of V_p = 3880 ($m\,s^{-1}$), V_s = 1860 ($m\,s^{-1}$), density = 920 ($kg\,m^{-3}$) were used in the model. The dirty ice is likely to contain about 5% debris, as discussed in the text, so the effect on the estimated bed properties is small.

(Table 2). As shown in Table 2, the estimated density of the subglacial sediments changes significantly with the assumed debris concentration of the overlying ice, but seismic velocities of the sediments are little affected over the range of debris concentrations in the ice than we consider likely. Thus, given the likelihood that there is debris-bearing ice at the base of the ice stream, the bed is probably somewhat more consolidated than would be estimated assuming clean ice to the bottom; however, the effect of the debris-bearing ice on estimated basal conditions is small and does not change the basic inference that basal conditions vary strongly, with some materials still relatively unconsolidated and thus likely soft.

6. Discussion

Our seismic survey was designed to study the base of the ice and its interaction with the substrate but provides enough evidence to show that the sticky spot is underlain by deeper sedimentary layers. From analogy to results of other studies in the region and from geologic understanding, the topographic high that underlies the sticky spot likely exists because of prior uplift linked to deeper structural control associated with the West Antarctic Rift System [e.g., *Rooney et al.*, 1991; *Muto et al.*, 2013; also see *Matsuoka et al.*, 2015; *Luthra*, 2017], and thus has been a persistent feature of the ice stream system.

The KIS subglacial hydrological potential map calculated assuming water pressure equal to ice overburden pressure (Figure 1d) shows that any water flowing from upstream is directed around both the sticky spot and the rest of our seismic line (Figure 1d). We note, however, that ice stream flow continues across a sticky spot on WIS that would similarly be isolated from water supply from upglacier if hydropotential were equal to the ice overburden pressure; however, seismic data for that WIS sticky spot indicate that dilated, lubricating till contributes to the continuing ice stream motion [*Luthra et al.*, 2016]. The likely explanation is that the WIS flow generates high shear stress on the sticky spot there, which lowers the hydropotential on the sticky spot and pumps lubricating water onto it, especially during the earthquakes that now enable most of the WIS motion (equivalent to the suction pump action at dilational fault jogs of tectonic earthquakes) [*Winberry et al.*, 2014; *Luthra et al.*, 2016]. At present, slow-moving KIS cannot similarly transfer stresses [*Walker et al.*, 2016] to drive large earthquakes that would pump water onto the sticky spot, but such behavior may have occurred in the past when KIS was active.

The most prominent difference in basal conditions between KIS and neighboring active ice streams including WIS is that the bed of KIS is more variable, with strong zones interspersed with weaker and potentially deformable ones. Our observations confirm earlier geophysical and borehole studies that portions of the bed of KIS remain soft, with high water pressure and weak, high-porosity tills. Interpretations of earlier seismic experiments on KIS that did not include the effects of debris in basal ice may have indicated tills somewhat weaker than actually exist, but even allowing for this, deformable tills still are known from borehole studies and geophysics. Unlike WIS, however, other portions of the bed of KIS are strongly consolidated or frozen, as shown by borehole observations [*Kamb*, 2001; *Engelhardt*, 2004] as well as geophysical data.

The results from the sticky spot on WIS likely are relevant. When an ice stream is moving rapidly, a local region of the bed cannot easily become dewatered or frozen, because stress transferred from surrounding regions will restore its motion, generating frictional heat or pumping in water to lubricate it. If the ice stream speed or water availability drops, however, then the ability to lubricate a sticky spot also drops, and beyond some threshold the ice stream may stop, as observed for KIS.

We next return to our inference of 40 m of frozen-on ice containing a low but nonzero concentration of debris (~5%) in the basal low at 6500 m on our survey. The weak reflector is clear in Figure 2. We lack additional parallel lines or crossing lines, and there is no borehole through the feature, so we cannot entirely exclude other hypotheses. We have attempted to construct models in which this feature results from an off-axis reflection or reflections, and have not found this to be likely; we consider it most likely that it is a channel oriented along the former ice stream flow direction and thus perpendicular to our survey line. We note that at least local occurrence of channelized subglacial water flow has been inferred for this general region of West Antarctica, based on data including observations of deglaciated regions in the Ross Sea [*Halberstadt et al.*, 2016] and on geophysical surveys near the modern grounding zone of Whillans Ice Stream [*Horgan et al.*, 2013].

The weak reflector is similar to reflectors observed elsewhere on our line. This similarity, together with the knowledge that debris-bearing ice is present in at least some places in our survey region [*Engelhardt*, 2004], argues for our interpretation of a contact between clean and debris-bearing ice. We have considered the possibility of a reflection from a change in *c* axis fabric and find it unlikely that such a transition would occur with the observed configuration; the locally low bed would not lead to concentrated deformation in the observed pattern of the reflector. Tectonic processes might have thickened an otherwise thinner layer; however, this layer occurs at a location where the bed is locally low, making it unlikely that compressive deformation would greatly thicken the ice. We do not believe that we can completely exclude any of these possibilities, but we do not favor them.

Freeze-on rates beneath the ice stream are generally limited by heat conduction into the ice and may be ~4 mm a^{-1} [*Engelhardt*, 2004; *Christoffersen et al.*, 2010]. At that rate, it would take 10,000 years to form a 40 m thick layer of ice; however, even local surface accumulation from snowfall on an isolated sticky spot would lead to steady flow that would move the ice away in that much time, and other possible flow patterns would move frozen-on ice away more rapidly. Hence, if this is frozen-on debris-rich ice that has not been greatly thickened by tectonic processes, faster accretion seems required in this region than in the surroundings. We hypothesize that this ice accreted in a basal channel through the "glaciohydraulic supercooling" process [*Lawson et al.*, 1998; *Alley et al.*, 1998; *Creyts and Clarke*, 2010].

In this scenario, the water flowing up an overdeepened bed is supercooled and subsequently freezes due to the increase in the pressure-melting temperature at the base of the ice, entraining sediment at low concentration [*Lawson et al.*, 1998, *Alley et al.*, 1998]. Typical outburst floods generate excess heat and melt ice, but those of the Siple Coast ice streams are quite slow [e.g., *Fricker et al.*, 2007; *Fricker and Scambos*, 2009; *Winberry et al.*, 2009] and may indeed occur in the supercooling field. Thus, we consider it possible, and worthy of further modeling, that lake drainages followed the channel across the flank of the sticky spot and perhaps into a surface low in the lee of the sticky spot, supercooling as they rose up the bed slope and accreting ice. Even with lake drainages, a considerable amount of time may have been required to accrete 40 m of ice, perhaps suggesting that the sticky spot and its channel were stable for some interval before the shutdown of KIS, and that the ice stream may have stopped moving rapidly across the sticky spot (or never moved rapidly?) before the adjacent ice stream slowed greatly. Much additional modeling would be required to test these speculations.

7. Conclusions

A seismic survey including amplitude analysis and imaging was completed across the main sticky spot near the center of KIS, West Antarctica. Interpretations guided by prior borehole and other studies reveal strong spatial variability of bed conditions. The sticky spot rests on a local topographic high composed of sedimentary layers. Any modern subglacial water flow is routed around the sticky spot if the hydropotential is close to the weight of the ice. The seismic data reveal a weak reflector that likely is the top of the debris-bearing ice documented in borehole observations; based on the strength of this reflector in our survey, debris concentration is probably low (~5%) in the seismically resolvable layer. Materials beneath the ice range from dilatant till to more-consolidated sediments, with a tendency for potentially deformable till to be in topographic lows and in the flat region off the edge of sticky spot, but with notable exceptions. In one location, a basal channel containing dilatant till is overlain by as much as 40 m of what we interpret to be frozen-on ice with a low but

nonzero debris concentration; we hypothesize that this represents accretion from glaciohydraulic supercooling of lake-drainage events routed along the channel when the ice stream was still active.

The great heterogeneity of the bed of KIS stands in marked contrast to the uniformity of the bed of adjacent WIS and other active ice streams. This likely represents the ability of a fast-moving ice stream to redistribute stress and lubricant, with heterogeneity emerging after KIS stopped. Water piracy or other loss of water likely contributed to the stoppage, with the sticky spot playing an active role in restraining the ice motion.

Acknowledgments

The funding for this work was provided by the National Science Foundation (NSF OPP grants 0086297 and 0226535) and the Center for the Remote Sensing of Ice Sheets (CRESIS). We thank the 2002–2003 OND field party (D. Voigt, P. Winberry, P. Braddock, R. Greschke, A. Morton, A. Mironov, S. O'Neel, and M. Nolan) for field acquisition of this data set. Additionally, we would like to thank John Anderson and an anonymous reviewer for greatly improving the quality of this manuscript. L.E. Peters acknowledges funding through the Australian Research Council's Special Research Initiative for Antarctic Gateway Partnership (Project ID SR140300001). The seismic data are available at the following address https://ds.iris.edu/ds/nodes/dmc/forms/assembled-data/?dataset_report_number=06-001.

References

Aki, K., and P.G. Richards (2002), *Quantitative Seismology*, 2nd ed., 704 pp., Univ. Sci. Books, Sausalito, Calif.

Alley, R. B. (1993), In search of ice-stream sticky spots, *J. Glaciol.*, *39*(133), 447–454.

Alley, R., D. Blankenship, C. Bentley, and S. T. Rooney (1986), Deformation of till beneath ice stream B, West Antarctica, *Nature*, *322*, 57–59.

Alley, R., D. Blankenship, C. R. Bentley, and S. T. Rooney (1987), Till beneath ice stream B: 3. Till deformation: evidence and implications, *J. Geophys. Res.*, *92*, 8921–8929, doi:10.1029/JB092iB09p08921.

Alley, R., S. Anandakrishnan, C. Bentley, and N. Lord (1994), A water-piracy hypothesis for the stagnation of Ice Stream C, Antarctica, *Ann. Glaciol.*, *20*(1), 187–194.

Alley, R. B., D. E. Lawson, E. B. Evenson, J. C. Strasser, and G. J. Larson (1998), Glaciohydraulic supercooling: A freeze-on mechanism to create stratified, debris-rich basal ice: II. Theory, *J. Glaciol.*, *44*(148), 563–569.

Anandakrishnan, S. (2003), Dilatant till layer near the onset of streaming flow of Ice Stream C, West Antarctica, determined by AVO (amplitude vs offset) analysis, *Ann. Glaciol.*, *36*(1), 283–286.

Anandakrishnan, S., and R. Alley (1994), Ice stream C, Antarctica, sticky spots detected by microearthquake monitoring, *Ann. Glaciol.*, *20*(1), 183–186.

Anandakrishnan, S., and R. Alley (1997a), Tidal forcing of basal seismicity of ice stream C, West Antarctica, observed far inland, *J. Geophys. Res.*, *102*, 15,183–15,196, doi:10.1029/97JB01073.

Anandakrishnan, S., and R. B. Alley (1997b), Stagnation of ice stream C, West Antarctica by water piracy, *Geophys. Res. Lett.*, *24*, 265–268, doi:10.1029/96GL04016.

Anandakrishnan, S., and C. Bentley (1993), Micro-earthquakes beneath Ice Streams B and C, West Antarctica: Observations and implications, *J. Glaciol.*, *39*, 455–462.

Anandakrishnan, S., R. Alley, R. Jacobel, and H. Conway (2001), The flow regime of Ice Stream C and hypotheses concerning its recent stagnation, in *The West Antarctic Ice Sheet: Behavior and Environment*, pp. 283–296, AGU, Washington, D. C.

Atre, S. R., and C. R. Bentley (1993), Laterally varying basal conditions beneath Ice Streams B and C, West Antarctica, *J. Glaciol.*, *39*(133), 507–514.

Bennett, M. R. (2003), Ice streams as the arteries of an ice sheet: Their mechanics, stability and significance, *Earth Sci. Rev.*, *61*(3), 309–339.

Bentley, C. R. (1971), Seismic evidence for moraine within the basal Antarctic ice sheet, in *Antarctic Snow and Ice Studies II*, pp. 89–129, AGU, Washington, D. C.

Bentley, C. R. (1972), Seismic-wave velocities in anisotropic ice: A comparison of measured and calculated values in and around the deep drill hole at Byrd Station, Antarctica, *J. Geophys. Res.*, *77*, 4406–4420, doi:10.1029/JB077i023p04406.

Bentley, C. R. (1987), Antarctic ice streams: A review, *J. Geophys. Res.*, *92*, 8843–8858, doi:10.1029/JB092iB09p08843.

Bentley, C. R., and H. Kohnen (1976), Seismic refraction measurements of internal friction in Antarctic ice, *J. Geophys. Res. 81*(8), 1519–1526, doi:10.1029/JB081i008p01519.

Bentley, C. R., N. Lord, and C. Liu (1998), Radar reflections reveal a wet bed beneath stagnant Ice Stream C and a frozen bed beneath ridge BC, West Antarctica, *J. Glaciol.*, *44*(146), 149–156.

Bindschadler, R. A., E. P. Roberts, and A. Iken (1990), Age of Crary Ice Rise, Antarctica, determined from temperature-depth profiles, *Ann. Glaciol.*, *14*, 13–16.

Bindschadler, R., P. Vornberger, D. Blankenship, T. Scambos, and R. Jacobel (1996), Surface velocity and mass balance of Ice Streams D and E, West Antarctica, *J. Glaciol.*, *42*(142), 461–475.

Blankenship, D. D., C. R. Bentley, S. Rooney, and R. B. Alley (1986), Seismic measurements reveal a saturated porous layer beneath an active Antarctic ice stream, *Nature*, *322*, 54–57.

Blankenship, D. D., C. Bentley, S. Rooney, and R. B. Alley (1987), Till beneath Ice Stream B: 1. Properties derived from seismic travel times, *J. Geophys. Res.*, *92*, 8903–8911, doi:10.1029/JB092iB09p08903.

Bougamont, M., S. Tulaczyk, and I. Joughin (2003), Response of subglacial sediments to basal freeze-on 2. Application in numerical modeling of the recent stoppage of Ice Stream C, West Antarctica, *J. Geophys. Res.*, *108*(B4), 2223, doi:10.1029/2002JB001936.

Bougamont, M., P. Christoffersen, S. Price, H. Fricker, S. Tulaczyk, and S. Carter (2015), Reactivation of Kamb Ice Stream tributaries triggers century-scale reorganization of Siple Coast ice flow in West Antarctica, *Geophys. Res. Lett.*, *42*, 8471–8480, doi:10.1002/2015GL065782.

Catania, G. A., H. B. Conway, A. M. Gades, C. F. Raymond, and H. Engelhardt (2003), Bed reflectivity beneath inactive ice streams in West Antarctica, *Ann. Glaciol.*, *36*(1), 287–291.

Christoffersen, P., S. Tulaczyk, and A. Behar (2010), Basal ice sequences in Antarctic ice stream: Exposure of past hydrologic conditions and a principal mode of sediment transfer, *J. Geophys. Res.*, *115*, F03034, doi:10.1029/2009JF001430.

Creyts, T. T., and G. K. C. Clarke (2010), Hydraulics of subglacial supercooling: Theory and simulations for clear water flows, *J. Geophys. Res.*, *115*, F03021, doi:10.1029/2009JF001417.

Engelhardt, H. (2004), Thermal regime and dynamics of the West Antarctic ice sheet, *Ann. Glaciol.*, *39*(1), 85–92.

Engelhardt, H., and B. Kamb (2013), Kamb Ice Stream flow history and surge potential, *Ann. Glaciol.*, *54*(63), 287–298.

Fricker, H. A., and T. Scambos (2009), Connected subglacial lake activity on lower Mercer and Whillans Ice Streams, West Antarctica, 2003–2008, *J. Glaciol.*, *55*(190), 303–315.

Fricker, H. A., T. Scambos, R. Bindschadler, and L. Padman (2007), An active subglacial water system in West Antarctica mapped from space, *Science*, *315*(5818), 1544–1548.

Fricker, H. A., M. R. Siegfried, S. P. Carter and T. A. Scambos (2016), A decade of progress in observing and modelling Antarctic subglacial water systems, *Philos. Trans. R. Soc. A*, *374*(2059), 20140294, doi:10.1098/rsta.2014.0294.

Halberstadt, A. R. W., L. M. Simkins, S. L. Greenwood, and J. B. Anderson (2016), Past ice-sheet behaviour: Retreat scenarios and changing controls in the Ross Sea, Antarctica, *Cryosphere*, *10*(3), 1003–1020.

Holland, C. W., and S. Anandakrishnan (2009), Subglacial seismic reflection strategies when source amplitude and medium attenuation are poorly known, *J. Glaciol.*, *55*(193), 931–937.
Horgan, H. J., R. B. Alley, K. Christianson, R. W. Jacobel, S. Anandakrishnan, A. Muto, L. H. Beem, and M. R. Siegfried (2013), Estuaries beneath ice sheets, *Geology*, *41*(11), 1159–1162.
Hulbe, C., and M. A. Fahnestock (2007), Century-scale discharge stagnation and reactivation of the Ross ice streams, West Antarctica, *J. Geophys. Res.*, *112*, F03S27, doi:10.1029/2006JF000603.
Iverson, N. R., and L. K. Zoet (2016), Experiments on the dynamics and sedimentary products of glacier slip, *Geomorphology*, *244*, 121–134.
Jacobel, R. W., B. C. Welch, D. Osterhouse, R. Pettersson, and J. A. MacGregor (2009), Spatial variation of radar-derived basal conditions on Kamb Ice Stream, West Antarctica, *Ann. Glaciol.*, *50*(51), 10–16.
Jacobs, S. S., A. Jenkins, C. F. Giulivi, and P. Dutrieux (2011), Stronger ocean circulation and increased melting under Pine Island Glacier ice shelf, *Nat. Geosci.*, *4*(8), 519–523.
Joughin, I. R., and R. B. Alley (2011), Stability of the West Antarctic ice sheet in a warming world, *Nat. Geosci.*, *4*(8), 506–513.
Joughin, I. R., S. Tulaczyk, R. Bindschadler, and S. F. Price (2002), Changes in West Antarctic ice stream velocities: Observation and analysis, *J. Geophys. Res.*, *107*(B11), 2289, doi:10.1029/2001JB001029.
Joughin, I. R., S. Tulaczyk, and H. F. Engelhardt (2003), Basal melt beneath Whillans ice stream and ice streams A and C, West Antarctica, *Ann. Glaciol.*, *36*(1), 257–262.
Joughin, I. R., R. Bindschadler, M. A. King, D. Voigt, R. B. Alley, S. Anandakrishnan, H. Horgan, L. Peters, P. Winberry, and S. B. Das (2005), Continued deceleration of Whillans ice stream, West Antarctica, *Geophys. Res. Lett.*, *32*, L22501, doi:10.1029/2005GL024319.
Joughin, I. R., B. E. Smith, and B. Medley (2014), Marine ice sheet collapse potentially under way for the Thwaites Glacier Basin, West Antarctica, *Science*, *344*(6185), 735–738.
Kamb, B. (2001), Basal zone of the West Antarctic ice streams and its role in lubrication of their rapid motion, in *The West Antarctic Ice Sheet: Behavior and Environment*, pp. 157–199, AGU, Washington, D. C.
Lawson, D. E., J. C. Strabser, E. B. Evenson, R. B. Alley, G. J. Larson, and S. A. Arcone (1998), Glaciohydraulic supercooling: A freeze-on mechanism to create stratified, debris-rich basal ice: I. Field evidence, *J. Glaciol.*, *44*(148), 547–563.
Leeman, J. R., R. D. Valdez, R. B. Alley, S. Anandakrishnan, and D. M. Saffer (2016), Mechanical and hydrologic properties of Whillans Ice Stream till: Implications for basal strength and stick-slip failure, *J. Geophys. Res. Earth Surf.*, *121*, 1295–1309, doi:10.1002/2016JF003863.
Luthra, T. (2017), Seismic investigation of sediments beneath Antarctic ice streams, PhD thesis, The Pennsylvania State Univ.
Luthra, T., S. Anandakrishnan, J. P. Winberry, R. B. Alley, and N. Holschuh (2016), Basal characteristics of the main sticky spot on the ice plain of Whillans Ice Stream, Antarctica, *Earth Planet. Sci. Lett.*, *440*, 12–19.
Matsuoka, K., R. C. A. Hindmarsh, G. Moholdt, M. J. Bentley, H. D. Pritchard, J. Brown, H. Conway, R. Drews, G. Durand, and D. Goldberg (2015), Antarctic ice rises and rumples: Their properties and significance for ice-sheet dynamics and evolution, *Earth Sci. Rev.*, *150*, 724–745.
Mouginot, J., E. Rignot, and B. Scheuchl (2014), Sustained increase in ice discharge from the Amundsen Sea Embayment, West Antarctica, from 1973 to 2013, *Geophys. Res. Lett.*, *41*, 1576–1584, doi:10.1002/2013GL059069.
Muto, A., K. Christianson, H. J. Horgan, S. Anandakrishnan, and R. B. Alley (2013), Bathymetry and geological structures beneath the Ross Ice Shelf at the mouth of Whillans Ice Stream, West Antarctica, modeled from ground-based gravity measurements, *J. Geophys. Res. Solid Earth*, *118*, 4535–4546, doi:10.1002/jgrb.50315.
Peters, L. E., and S. Anandakrishnan (2007), Subglacial conditions at a sticky spot along Kamb Ice Stream, West Antarctica, in *Antarctica: A Keystone in a Changing World-Online Proceedings of the 10th ISAES*, edited by A. K. Cooper et al., *U.S. Geol. Surv. Open File Rep., 2007-1047*, 5 p.
Peters, L. E., S. Anandakrishnan, C. W. Holland, H. Horgan, D. D. Blankenship, and D. Voigt (2008), Seismic detection of a subglacial lake near the South Pole, Antarctica, *Geophys. Res. Lett.*, *35*, L23501, doi:10.1029/2008GL035704.
Price, S. F., R. Bindschadler, C. L. Hulbe, and I. R. Joughin (2001), Post-stagnation behavior in the upstream regions of Ice Stream C, West Antarctica, *J. Glaciol.*, *47*(157), 283–294.
Rathbun, A. P., C. Marone, R. B. Alley, and S. Anandakrishnan (2008), Laboratory study of the frictional rheology of sheared till, *J. Geophys. Res.*, *113*, F02020, doi:10.1029/2007JF000815.
Retzlaff, R., and C. R. Bentley (1993), Timing of stagnation of Ice Stream C, West Antarctica, from short-pulse radar studies of buried surface crevasses, *J. Glaciol.*, *39*, 553–561.
Rignot, E., J. L. Bamber, M. R. Van Den Broeke, C. Davis, Y. Li, W. J. Van De Berg, and E. Van Meijgaard (2008), Recent Antarctic ice mass loss from radar interferometry and regional climate modelling, *Nat. Geosci.*, *1*(2), 106–110.
Rignot, E., J. Mouginot, and B. Scheuchl (2011), Ice flow of the Antarctic ice sheet, *Science*, *333*(6048), 1427–1430.
Robel, A., C. Schoof, and E. Tziperman (2014), Rapid grounding line migration induced by internal ice stream variability, *J. Geophys. Res. Earth Surf.*, *119*, 2430–2447, doi:10.1002/2014JF003251.
Roethlisberger, H. (1972), *Seismic Exploration in Cold Regions*, *Monograph II A2a*, US Army CRREL, Hanover, N. H.
Rooney, S. T., D. D. Blankenship, R. B. Alley, and C. R. Bentley (1991), Seismic reflection profiling of a sediment-filled graben beneath ice stream B, West Antarctica, in *Geological Evolution of Antarctica*, edited by M. R. A. Thomson, J. A. Crame, and J. W. Thompson, pp. 261–265, Cambridge Univ. Press, Cambridge.
Shepherd, A., E. R. Ivins, A. Geruo, V. R. Barletta, M. J. Bentley, S. Bettadpur, K. H. Briggs, D. H. Bromwich, R. Forsberg, and N. Galin (2012), A reconciled estimate of ice-sheet mass balance, *Science*, *338*(6111), 1183–1189.
Smith, A. (1997), Basal conditions on Rutford ice stream, West Antarctica, from seismic observations, *J. Geophys. Res.*, *102*, 543–552, doi:10.1029/96JB02933.
Tulaczyk, S., W. B. Kamb, and H. F. Engelhardt (2000), Basal mechanics of ice stream B, West Antarctica: 1. Till mechanics, *J. Geophys. Res.*, *105*, 463–481, doi:10.1029/1999JB900329.
van der Wel, N., P. Christoffersen, and M. Bougamont (2013), Dynamic response of ice streams to switches in subglacial water-flow paths, paper presented at EGU General Assembly Conference Abstracts.
Vogel, S., S. Tulaczyk, B. Kamb, H. Engelhardt, F. Carsey, A. Behar, A. Lane, and I. Joughin (2005), Subglacial conditions during and after stoppage of an Antarctic Ice Stream: Is reactivation imminent?, *Geophys. Res. Lett.*, *32*, L14502, doi:10.1029/2005GL022563.
Walker, R. T., B. R. Parizek, R. B. Alley, and S. M. J. Nowicki (2016), A viscoelastic model of ice stream flow with application to stick–slip motion, *Front. Earth Sci.*, *4*(2), 11, doi:10.3389/feart.2016.00002.
Winberry, J. P., S. Anandakrishnan, and R. B. Alley (2009), Seismic observations of transient subglacial water-flow beneath MacAyeal Ice Stream, West Antarctica, *Geophys. Res. Lett.*, *36*, L11502, doi:10.1029/2009GL037730.
Winberry, J. P., S. Anandakrishnan, R. B. Alley, D. A. Wiens, and M. J. Pratt (2014), Tidal pacing, skipped slips and the slowdown of Whillans Ice Stream, Antarctica, *J. Glaciol.*, *60*(222), 795–807.